Contents lists available at ScienceDirect

Process Safety and Environmental Protection

journal homepage: www.elsevier.com/locate/psep

# A novel MD-ZVI integrated approach for high arsenic groundwater decontamination and effluent immobilization

*Olusegun K. Abass*[a,*], *Teng Ma*[a,**], *Shuqiong Kong*[a,b], *Zhiqiang Wang*[a], *Martin T. Mpinda*[a]

[a] *School of Environmental Studies and State Key Laboratory of Biogeology and Environmental Geology, China University of Geosciences, Wuhan 430074, PR China*

[b] *Department of Soil, Water and Environmental Science, University of Arizona, Tucson, AZ 85721, United States*

ARTICLE INFO

*Article history:*
Received 16 December 2015
Received in revised form 2 March 2016
Accepted 11 March 2016
Available online 17 March 2016

*Keywords:*
Acid-purged ZVI
Arsenic adsorption/reduction
DCMD-APZ
Direct contact membrane distillation
Distillate flux
Groundwater contamination

ABSTRACT

A highly effective novel system of direct contact membrane distillation (DCMD) integrated with acid-purged zero-valent iron (APZ) technology has been developed. Compared to conventional processes of arsenic removal which reconstitute secondary contamination at disposal site, this system proves capable of simultaneous removal and immobilization of arsenic from contaminated water with great efficiency and improved water flux. Using composite microporous membranes of polytetrafluoroethylene (PTFE) and polypropylene (PP) integrated with APZ in a DCMD-APZ configuration, varying residual arsenic concentrations were injected anoxically into ≤2 g acid-washed Fuchen (XK 13-201) reduced Fe powder at a flow rate of 0.33 mL/min and pH 6 ± 1.0 at 60 °C. Results from this unique configuration show advantages including maximum distillate flux production of 55.5 kg/m$^2$ h with greater than 95% arsenic rejection efficiency using PTFE/PP composite membrane, fast adsorption and immobilization of rejected arsenic on APZ at $t_{1/2} \leq 30$ min, and electrochemical reduction of As(V) and/or As(III) to sparsely soluble As(0) as confirmed by macroscopic wet chemistry, adsorption kinetic model and X-ray photoelectron spectroscopic (XPS) analysis conducted within 5 days of experimental period. Since the arsenic adsorption/reduction process is a thermodynamically assisted phenomenon, integrated configuration of the DCMD-APZ technology stands out as a promising technique to mitigate the unresolved challenges of arsenic contamination and re-dissolution in groundwater.



## 1. Introduction

Arsenic (As), a well-known carcinogen found in groundwater or localized environments at high concentrations due to natural geo-accumulation processes or as a result of specific release from metal smelting operations, chemical spills and microbial mediated processes, has generated severe health concerns around the globe. As connoted from the Greek word arsenikon, arsenic has been attributed to being the "king of poison" (Vahidnia et al., 2007; Wang et al., 2012). Therefore, long-term exposure to high levels of As in drinking water has been associated with various skin lesions, cardiovascular diseases, diabetes, neuropathies, as well as cancers of several organs (Mazumder et al., 1998; Balakumar and Kaur, 2009; Navas-Acien et al., 2008; Mukherjee et al., 2003). Arsenic contamination in drinking water continues to stir concern

* *Corresponding author.*
** *Corresponding author.* Tel.: +86 27 62925561.
E-mail addresses: segunabass1@gmail.com (O.K. Abass), mateng@cug.edu.cn (T. Ma).
http://dx.doi.org/10.1016/j.psep.2016.03.007

internationally, due to its widespread distribution. This problem is particularly prevalent in Datong Basin, China where new endemic areas are constantly emerging.

Thus, it is highly desirable to develop approaches that can significantly improve the remediation of this class of contaminants in the environment; as such, integrated use of membrane purification technologies hold promises (Yang et al., 2014). Polymer and inorganic membranes have been essentially utilized for various filtration processes including chlorinated compounds and heavy metals removal, such as arsenic (Wang and Chung, 2013; Yarlagadda et al., 2011). Studies on As removal using membrane distillation (MD), a thermally driven process involving movement of vapor across a microporous hydrophobic membrane, have been well researched (Pal and Manna, 2010; Yarlagadda et al., 2011; Jadhav et al., 2015). Among the different kinds of MD process, direct contact membrane distillation (DCMD) is the most efficient and easy to utilize MD technique. Advances in this field include fabrication of hybrid membrane with higher rate of contaminants rejection, longevity and less fouling capabilities (Wang and Chung, 2015; Wang et al., 2015). Yet, there is a huge knowledge gap between the emergence and application of membrane distillation technique for arsenic groundwater remediation and lack of an adequate understanding of the process enhancement still exists.

Furthermore, recent research on high performance membranes based on carbon nanotubes reveals a distinctive 3D nanostructure that efficiently adsorbs arsenic from contaminated groundwater due to protected agglomeration, increased surface-to-volume ratio, and water pathway of 3D nanostructures (Vadahanambi et al., 2013). However, the commercial viability of this new class of thin-film composite membranes for water re-use hinges on the development of inexpensive coatings, chemistries and scalable processing methods that can reproducibly achieve the desired membrane structure and yield reasonable fluxes (Shannon et al., 2008). While these advances are plausible, treatment of residual arsenic currently lags behind in all available membrane applications for arsenic containment.

Increasing research efforts have focused on using various adsorbents such as Fe binary oxides (Kong et al., 2014) and zero valent iron (ZVI) to remove As (Farrell et al., 2001; Kanel et al., 2005; Ramos et al., 2009; Li et al., 2015; Baikousi et al., 2015), and have demonstrated that ZVI is an effective sorbent which may be used to immobilize As from groundwater via surface adsorption/complexation, reduction, surface precipitation or co-precipitation (Mak et al., 2009; Noubactep, 2008). However, there are limitations in the use of ZVI to remediate As in water. These include competition from other oxyanions such as phosphate and silicate for sorption sites at corroded iron surfaces and possible later release of sequestered As due to subsequent mineralogical transformation of initially formed corrosion products (Su and Puls, 2004). Controversies about the mechanisms for removal of arsenic especially regarding redox reactions are an ongoing issue. The rate and extent of As(V) reduction by ZVI may depend on the prevailing experimental conditions. For instance, some authors have argued that the contaminants enmeshed in the matrix of iron corrosion products are stable for long time under environmental conditions whether they are chemically transformed or not (Noubactep, 2006; Lackovic et al., 2000). The current concept on the microbial reduction of ferrihydrite or iron corrosion products in situ/ex situ, resulting in the release of adsorbed species (e.g. arsenic) raises questions about the immobilization status of adsorbed contaminants (Yadav et al., 2015; Huang et al., 2015).

Considering the foregoing, treatment of arsenic contaminated water by employing the efficiency of membrane filtration processes coupled with residual arsenic containment technologies could be a hot direction for future research. In view of this, the objectives of this study were to (1) introduce a highly effective novel system of direct contact membrane distillation (DCMD) integrated with acid-purged zero-valent iron (APZ) technology, (2) evaluate the different mechanisms essential for optimization of the DCMD process in the context of high arsenic groundwater, and (3) investigate the efficiency of DCMD-APZ technique for simultaneous high feed-As rejection and residual arsenic containment respectively. Most studies have utilized ZVI and modified reduced iron for adsorptive removal of arsenic under aerobic and anoxic conditions but little is known about the mechanism of arsenic removal in pump-and-treat method under simulated rigorous anoxic conditions. To the best of our knowledge, no study has reported the containment of residual arsenic generated from membrane treatment processes which are potential sources of secondary pollution. Hence, this study sheds light on the advantage the DCMD-APZ technology offers for efficient arsenic contaminant removal and immobilization.

## 2. Experimental

### 2.1. Materials and methods

Acrylonitrile butadiene styrene (ABS), a terpolymer of acrylonitrile, butadiene and styrene, was purchased from Saipwell (Shanghai, China) and used for the design of a lab-made module with dimension 28 cm × 19.5 cm × 6.5 cm, in the DCMD set-up. We obtained three hydrophobic flat-sheet membranes from Membrane Solutions LLC (Shanghai, China) and they were put to use without further treatment. Properties of each membrane are summarized in Table 1. Properly preserved groundwater samples obtained from Datong Basin in Shanxi Province, China (groundwater characteristics are presented in Table 2) and arsenic simulated solutions prepared using analytical reagent grade of $Na_2AsO_4{\cdot}7H_2O$ (Sinopharm Chemical Reagent Co. Ltd., China) for As(V) and $NaAsO_2$ (Sigma–Aldrich) for As(III) were used in the experiments. All chemical reagents utilized including HCl, NaOH, and NaCl are of analytical reagent grade. Deoxygenated ultra-pure water purge with high purity nitrogen gas at 70 °C for 4 h was employed in the APZ reaction process. This was done to simulate rigorous anoxic conditions found in groundwater environments and to eliminate dissolved $O_2$, a potential oxidant in these solutions.

### 2.2. Acid-purged ZVI synthesis

Zero valent iron (XK 13-201) obtained from Tianjin Fuchen Reagent Co. Ltd., China, with bulk iron composition of Fe – 98%,

**Table 1 – Membrane characteristics.**

| Membrane type | Active layer | Substrate layer | Nominal pore size (μm) | Porosity (%) | Thickness (μm) |
|---|---|---|---|---|---|
| PTFE0221 | PTFE | PP | 0.22 | 82 | 170 |
| PTFE0221B | PTFE | PET | 0.22 | 80 | 160 |
| MSPP270045 | PP | PET | 0.45 | 75 | 160 |

**Table 2 – Some applicable characteristics of groundwater chemistry used in this study (from Datong Basin, North China).**

| Composition/characteristics | Concentration range (mg/l) |
|---|---|
| Total As | 0.025–1.8 |
| Fe | 0.06–0.93 |
| Mg | 7.3–74.4 |
| Mn | <0.1–0.31 |
| Ca | 5.1–32.9 |
| Na | 46.1–339.3 |
| $HCO_3^-$ | 252–700 |
| pH | 7.2–9.1 |
| Eh | −144.7–173.9 |
| Ec (μS/cm) | 385.5–3730.0 |
| $SO_4^{2-}$ | 0–395 |
| $HS^-$ | 1–38 |

S – 0.06%, N – 0.005%, Cu – 0.0005%, and other minor impurities (less than 0.0003%) was used for the synthesis of acid-purged ZVI (APZ). The grain size, specific surface area and particle density of the reduced iron powder were 0.04–0.18 mm, 3.56 $m^2$/g, and 2.34 g/$cm^3$ respectively. 40 ml of 2 M HCl was added to 40 g of the reduced iron powder and aerated for 2 h; the mixture was washed thrice with deoxygenated ultra-pure water (Heal force, NW 15 UV) and dried for approximately 12 h at 60 °C in the oven. It is generally believed that the oxidative dissolution of ZVI can improve its contaminant sequestration ability (Triszcz et al., 2009). Therefore, exposure of APZ to $O_2$ during the pretreatment process leads to generation of $Fe^{2+}$ reaction products. However, due to the limited stability of $Fe^{2+}$ and its high sensitivity to $O_2$, it readily converts to $Fe^{3+}$ which subsequently forms oxides including magnetite, ferric oxy-hydroxides, and iron(III)hydroxides, when hydrolyzed (Mielczarski et al., 2005; Aleksanyan et al., 2007). Hence, processes geared toward the accelerative corrosion of ZVI surface can increase its contaminant removal characteristics. APZ samples produced were carefully sealed and immediately transferred for storage in the anaerobic chamber until use (Coy Laboratory Products, Inc., Model 10 Gas Analyzer).

Purging ZVI with acid (APZ) promotes the reactivity of ZVI and enables the disruption of the adherent iron oxide film (Lai and Lo, 2008), producing a highly porous oxidized iron shell that could facilitate transport of reducing species from the iron core where the redox potential is low enough to reduce the contaminant species under inert atmosphere. Possible increase in surface area of ZVI by washing in acid has also been documented (Alowitz and Scherer, 2002). Similarly, the APZ produced in this study also contains intermediate magnetite (see Fig. 5b), a strong reducing agent capable of reducing arsenate to arsenite and metallic arsenic as proposed by Sun et al. (2011).

### 2.3. *DCMD-APZ module set-up*

In the set-up, inlet and outlet distribution flow channels were drilled on both width sides of the upper and lower compartment of the module to ensure an even flow across the membrane. Experimental errors associated with operational variation between feed samples, and membrane handling was reduced by attaching adjustable siphons to module flow channels. The experimental set-up for the DCMD-APZ operation is schematically illustrated in Fig. 1. The structure and composition of this novel hybrid treatment set comprise five major units – the membrane module, hot and cold water bath for feed and distillate retention, respectively, peristaltic pumps compartment, feed and distillate flow regulating compartments and an anaerobic chamber for residual feed treatment.

In the DCMD approach, hot As-feed was channeled through the lower boundary of each membrane (listed in Table 1) while the cold distillate stream was designed to run in countercurrent direction to the feed flow on the upper side of the membrane in a cross-flow mode. During the experiments, As-feed water (both groundwater sample obtained from the field and simulated arsenic aqueous solutions) at varying temperatures, flow rates and concentrations were circulated through the set-up and the weight variation of the distillate flux in receiving tank was quantified using an electronic weighing balance. The effective membrane surface area designed to fit the lab-made module is 0.0538 $m^2$. Digital thermometers were used to monitor the module inlet and outlet temperature streams and a dial pressure gauge was employed to monitor the pressure of both streams. High concentrations of residual arsenic feed (generated on the feed side after the production of arsenic-free distillate flux) were channeled through a flow compartment attached tightly to the anaerobic compartment comprising a set of batch reactors with varying doses of APZ samples. Distillate samples collected at equal intervals were analyzed to determine the arsenic concentrations using hydride-generation atomic fluorescence spectrometry (HG-AFS) (AFS-9130, Titan, China) according to the procedure described by Sanchez-Rodas et al. (2010).

Arsenic removal efficiencies of the different membranes were carried out. As-feed solution pH was not controlled as the system removes contaminants effectively irrespective of the solution pH (Hou et al., 2010). Prior to starting the experiment, seepages were checked and measurements were taken after the system stabilizes to avoid experimental errors. The experiments were discontinued after several hours of operation to prevent distillate production exceeding levels that are way higher than the maximum contaminant limit (MCL) of arsenic in drinking water systems. The feed temperature was varied between 50 °C and 80 °C with the aid of a thermostatic water bath to study the influence of feed inlet temperature on flux at each run. Further, flow rates of the hot and cold streams were varied between 0.22 and 0.76 L/min, and between 0.85 and 1.30 L/min respectively. This was achieved by adjusting the peristaltic pumps and flow meters. Using raw contaminated arsenic water from Datong Basin, China at concentration range of 0.025–1.8 mg/l (Table 2) and simulated As-feed concentrations between 0 and 20 mg/l for As(V), and between 0 and 2.3 mg/l for As(III), we estimated the effect of arsenic concentration on flux and distillate quality after approximately 5 days of experimental runs.

### 2.4. *Batch experiments*

Hot residual As-feed discharge tube was connected to batch reactors arranged in series at a flow rate of 0.33 mL/min at 60 °C and add up to a volume of 30 ml. A predetermined optimum dosage of 2 g APZ was used in each reactor sample mix, purged for 5 min with $N_2$ after pH of the solutions was adjusted between 6.0 ± 1.0 using appropriate amounts of buffer solution (HCl and NaOH) and then capped. The redox potential (Eh) at each reactor was measured at the start and end of each run. Separate arsenic reduction experiment was carried out in a 30 ml reaction vial by successive additions of 15 ml deoxygenated ultra-pure water, 2.0 g APZ, and 15 ml As(V) solution with initial concentration of 0.5 mg/l (all reactions

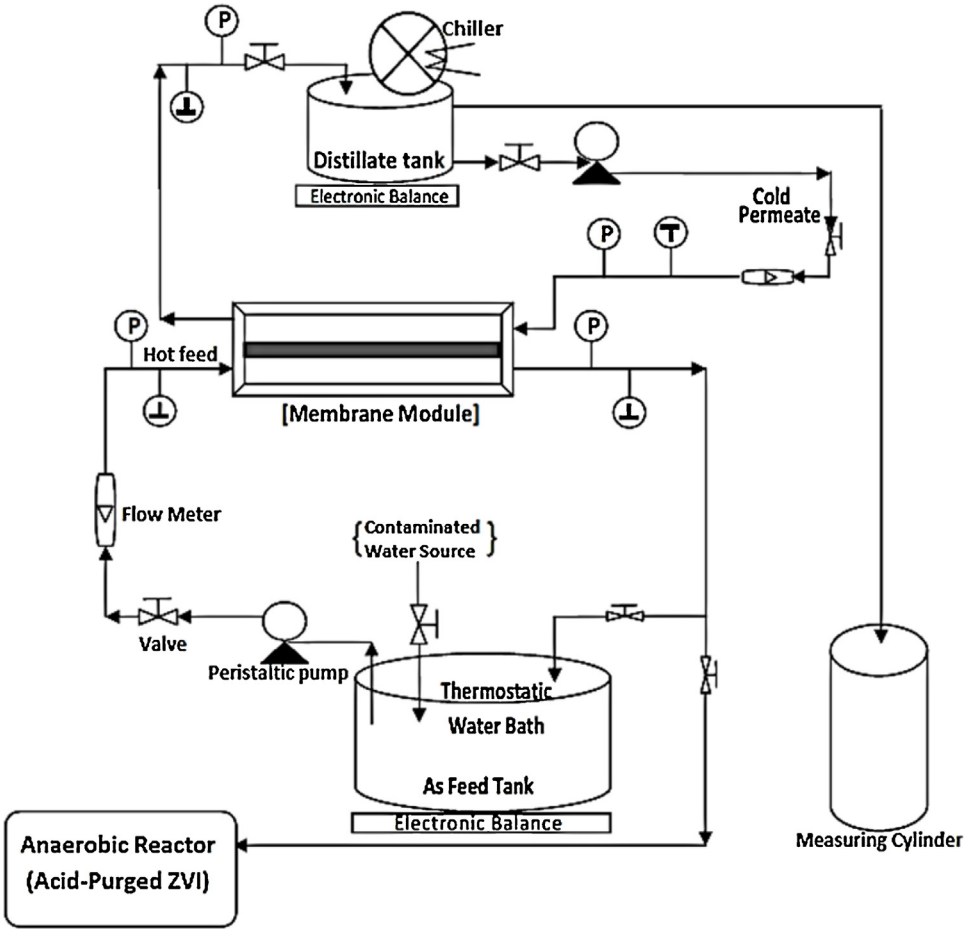


**Fig. 1 – DCMD-APZ schematic diagram for simultaneous removal and immobilization of arsenic contaminants (P – pressure sensor and T – thermometer).**

were conducted under strict anoxic condition). The solution pH was adjusted before the addition of APZ and was agitated at 230 rpm at varying times with THZ-C DRAGONLAB shaker at 30–40 °C. Suspension samples from both the batch reactors and reaction vials were extracted by syringe inserted through the lid of the reactors and acidified to dissolve any formed precipitate before subsequent measurement of total arsenic and sorbed As(III)/As(V) concentrations. Soluble/dissolved arsenic was determined after extraction with 0.22 μm filters. Adsorbed arsenic on APZ was measured using the difference between the initial and total arsenic concentrations in the water samples (without filtration). Filters were used to determine the soluble arsenic concentration, distinguishing it from arsenic removal on APZ. Arsenic sorption capacity for APZ was also evaluated and arsenic speciation cartridge (CNW Technologies, USA) was used for selective removal of arsenate.

### 2.5. *Materials surface characterization*

Structural changes in the membranes surface after DCMD treatment were analyzed using Scanning Electron Microscopy (SEM) (Hitachi, S-3400N). Both fresh and used membrane samples were dried at atmospheric temperature before investigation. The samples were sputter-coated with gold to compensate for charge conduction and then examined at an accelerating voltage of 20 kV. Similarly, three-dimensional images of APZ particle shapes and surfaces were visualized using SEM, and the bulk elemental compositions were analyzed with an Energy Dispersive analysis of X-ray (EDAX) (FEI Quanta 200, Netherlands). Structures of surface precipitates on fresh ZVI and APZ (before treatment with arsenic solutions) were determined using X-ray Diffraction (XRD) obtained on Bruker D8 Advance (Germany) with CuK radiation.

Surface sensitive quantization of elements speciation on spent APZ was performed under inert atmosphere using X-ray Photoelectron Spectroscopy (XPS) on a Thermo Electron VG Multilab 2000 (USA) that uses non-monochromatic A1 Kα1.2 radiation (300W PE 25 eV). Step sizes of 1.00 and 0.05 eV were used for the survey and high-resolution scans respectively. Low-energy electron flooding for charge compensation was applied and the takeoff angle was set at 90°, because the APZ sample was in powdered form and the depth of the samples analyzed was approximately 5 nm. The magic angle was adjusted to approximately 55°. The type of the surface precipitates formed was evaluated by finding the binding energy of the peaks of the XPS spectra (Bomben et al., 1995).

### 2.6. *DCMD model experiment*

In a typical DCMD process, mass transfer occurs from differences in temperature between hot feed and cold distillate flows. The two flows are separated by hydrophobic microporous membrane of thickness, $\delta m$ creating two boundary layers with distinct characteristics thickness as shown in Fig. 2.

The vapor pressure gradient created at the feed side of the membrane and distillate constitutes the main driving force for mass transfer through the membrane. However,

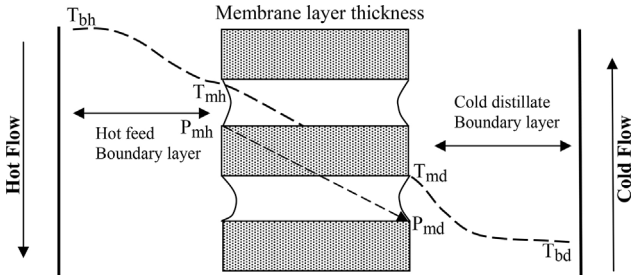


**Fig. 2 – Temperature polarization and mass transfer in DCMD process.**

heat transfer is limited by the hot boundary layer which produces resistance to heat flow and reduces water vapor flux across the membrane (Martinez-Diez and Vazquez-Gonzalez, 1999). This occurrence is caused by temperature polarization effect (TPE). Decrease in feed temperature is often associated with TPE, causing bulk hot feed temperature ($T_{bh}$) to change to $T_{mh}$ (temperature at the feed-membrane interface). Bulk distillate/permeate temperature ($T_{bd}$) increases progressively toward the distillate-membrane interface ($T_{md}$) as observed by Khayet et al. (2004). Negative effect on flux due to decrease in thermal driving force between the hot and cold boundary layers is associated with TPE which can be measured using the below equation:

$$\mathrm{TPE} = \frac{T_{mh} - T_{md}}{T_{bh} - T_{bd}} \tag{1}$$

In DCMD systems, an efficient fluid dynamics layout will cancel out the effect of TPE and yield high mass transfer across the membrane. However, TPE slants to zero for poorly designed system but this could be reduced under improved mixing conditions (Schofield et al., 1990). The vapor pressure difference across the dry porous membrane is represented by $P_{mh} - P_{md}$. For ideal solution, pure fluid saturation pressure ($P_s$) above a flat liquid surface could be determined by the Antoine equation (Wichterle and Linek, 1971):

$$P_s^c(T) = e^{K(A/(C+T))} \tag{2}$$

where $P_s^c(T)$ is the saturated vapor pressure of pure compound 'c' measured in Pascal at temperature $T$; and $K$, $A$ and $C$ are constants. Values of these constants for water are 23.1964, 3816.44 and −46.13 respectively (Wichterle and Linek, 1971). The water vapor pressures, $P_{mh}$ and $P_{md}$ at $T_{mh}$ and $T_{md}$, are a function of temperature, and are related to the activity of a solution. Optimization of the various modeling factors helped to achieve maximum recovery of distillate flux.

### 2.6.1. *Arsenic rejection efficiency*

The arsenic rejection efficiency ($R_{As}$ %) was calculated using the equation:

$$R_{As}(\%) = \frac{F_{conc.} - D_{conc.}}{F_{conc.}} \times 100\% \tag{3}$$

$F_{conc.}$ and $D_{conc.}$ are the feed and distillate arsenic concentration respectively. The distillate weight difference at definite time interval was used for the calculation of the flux across the membrane following the given experimental condition. The flux in kg/m$^2$ h was computed using the below formula:

$$J_i = \left(\frac{\Delta D_w}{M_a \cdot t}\right) \tag{4}$$

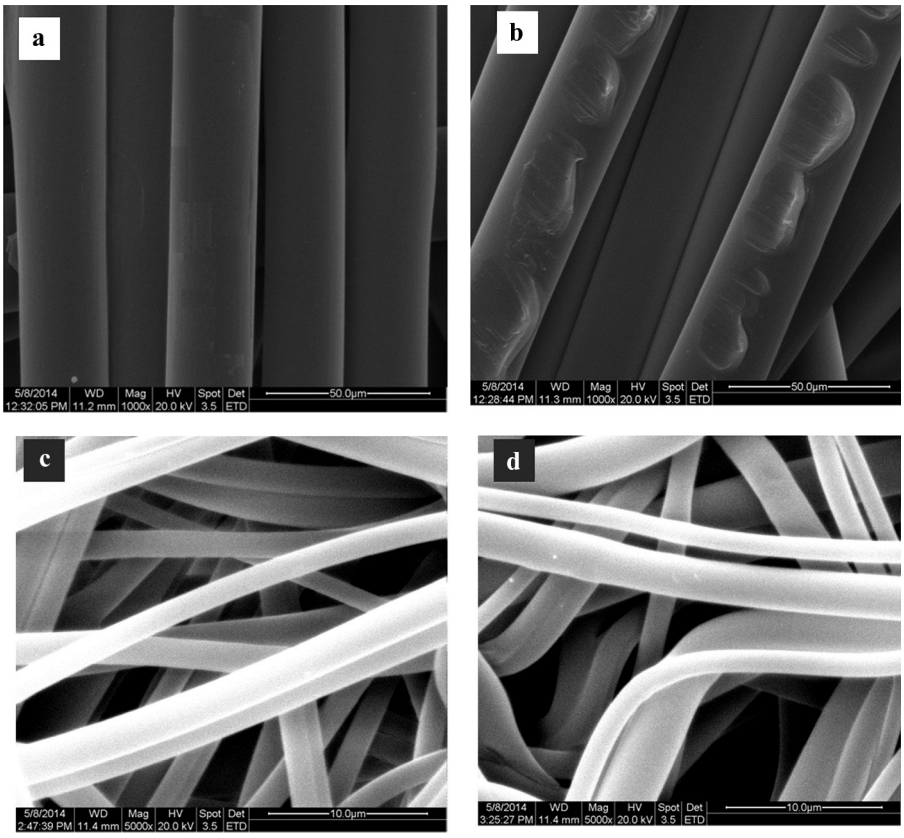


**Fig. 3 – SEM micrographs of inner surfaces of PTFE0221 and MSPP270045 membranes: (a) fresh PTFE0221, (b) used PTFE0221 after 120 h operation, (c) fresh MSPP270045 and (d) used MSPP270045 after 120 h operation.**

$J_i$ is the water or distillate flux, $\Delta D_w$ is the change in distillate weight at definite time interval, $M_a$ is the membrane surface area and t is the interval time in hours.

## 3. Results and discussion

### 3.1. *Characterization studies*

Electron micrographs of the PTFE0221, PTFE0221B and MSPP270045 membranes were acquired before and after arsenic removal experiments using Scanning Electron Microscopy analysis (Fig. 3). Micrographs of the used membranes displayed slight changes in morphology at the inner surface. Minimal changes in pore length, width and area of the membranes were observed after running the experiment for 5 days. Contrast between the unused and used PTFE0221(B) and MSPP270045 membranes in this study revealed obvious characteristics difference such as the formation of fragments on the used PTFE0221(B) membranes, which were not found on the fresh ones (Fig. 3a and b). In a study conducted by Barbe et al. (2000), they reported that morphological changes found in PP membranes after use were as a result of pore incursion by liquid flow, which generated a pressure regime causing the adjacent smaller pores to reduce in size and perhaps close entirely. These changes were observed directly on the thread-like structure of used PTFE0221(B) suggesting that physical force created between the membrane interface and feed solution could be the main reason for the distortion.

Unlike the PTFE0221(B) membranes, the pore sizes of the MSPP270045 membranes were significantly affected during the repeated mass transfer procedures, as water vapor diffuse from regions of dense pore concentrations to less dense regions (Fig. 3c and d). This raised the transfer resistance and resulted in frequent collision of water molecules, a

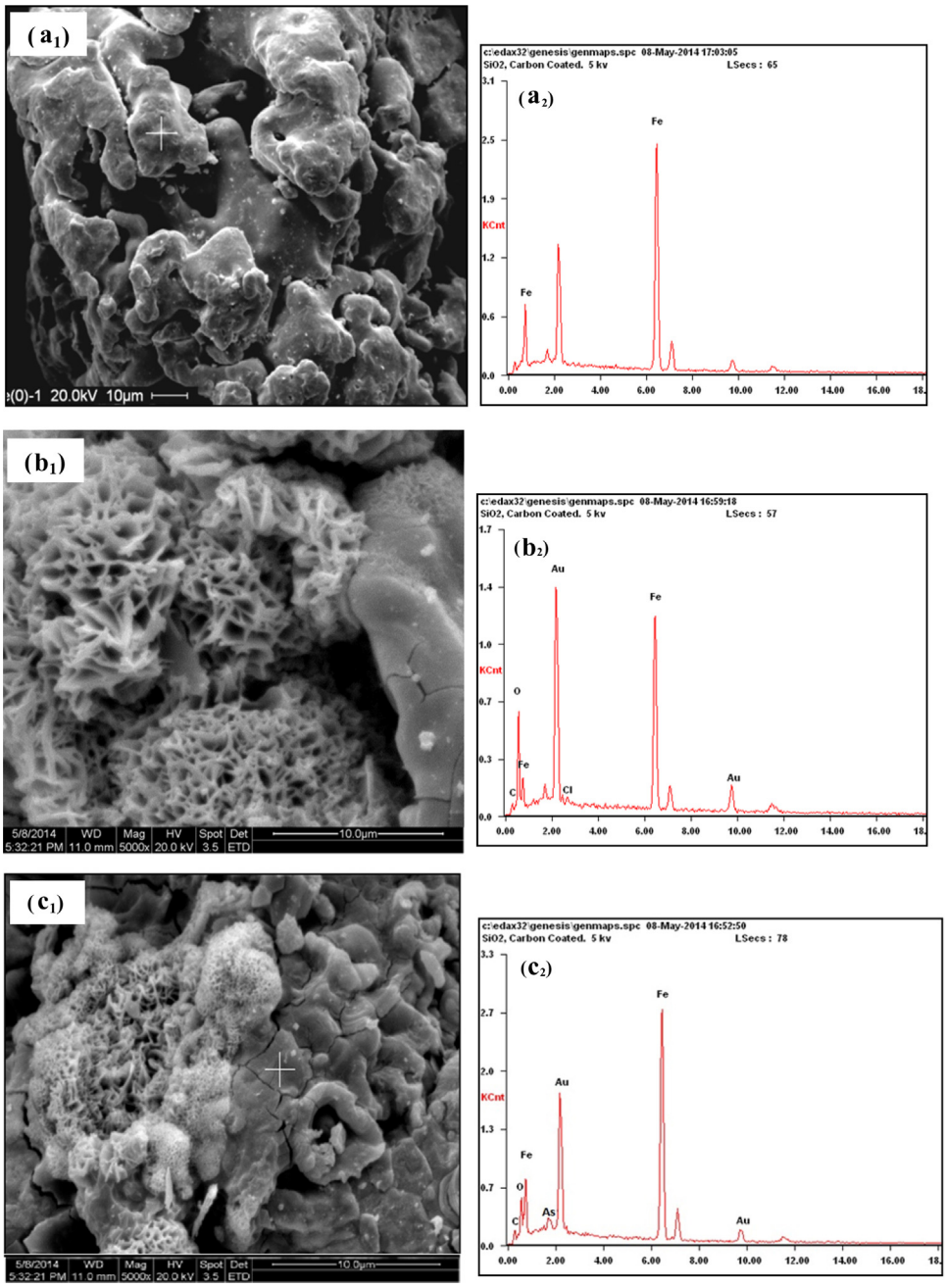


**Fig. 4 – SEM spectra of ($a_1$) Fresh ZVI, ($b_1$) APZ sample, ($c_1$) APZ treated with As(V) after 5 days and EDX peak analysis for ($a_2$) Fresh ZVI, ($b_2$) APZ sample, ($c_2$) APZ treated with As(V).**

phenomenon also observed by Qu et al. (2009). Approximately 120 h tests were conducted to evaluate the effect of fouling on the membranes. SEM images of all used membranes showed the absence of organic or inorganic stains after the 5 days operation except for MSPP270045 membrane which shows very minimal percentage of inorganic fouling (Fig. 3d). Throughout the experiment, the permeability and hydrophobicity of the used PTFE0221, PTFE0221B and MSPP270045 membranes were not altered even though there were slight morphological variations observed.

SEM images and EDX spectra of solid samples obtained from ZVI and 0.5 mg/l As-treated APZ after 5 days are shown in Fig. 4a–c. From the analysis, we observed that adsorption of arsenic with time resulted in increased particle aggregation stemming from iron(III)oxide/hydroxide precipitation. Further evidence from SEM micrograph of APZ shows clearly the growth of an amorphous crystallite phase, which transforms to an apparent spongy-like/flower-like semi-crystallite phase after reaction with As(V) solution (Xie et al., 2014). These semi-crystallite structures are known to be dynamically unstable and eventually dissolve to be replaced by steadier phases following the Ostwald ripening rule (Kanel et al., 2005). Quantitative SEM-EDX peak area analysis shows the presence of arsenic sorbed onto APZ surface up to 1% (wt.) over 5 days (Fig. 4c). The EDX peak area analysis provides an approximate surface corrosion product of elemental ratio Fe:O:As in order of abundance after 5 days.

Powdered samples of ZVI and APZ characterized using XRD are shown in Fig. 5a and b. Few sharp peaks were observed on X-ray diffractogram of APZ which corresponds to crystalline forms of magnetite, a strong electron donor and an effective absorbent for arsenic removal (Mayo et al., 2007). Reports from previous studies have shown that ZVI possess an oxide surface coating with inner and outer magnetite, maghemite layers respectively (Deng et al., 2006). The cubic structure obtained in this analysis could either be magnetite or maghemite. However, using a typical step scan angle and deconvoluting the peaks obtained with the aid of JADE program, the low angle peak detected was assigned to magnetite, while the ones at a higher angle can be assigned to maghemite. Moreover, the

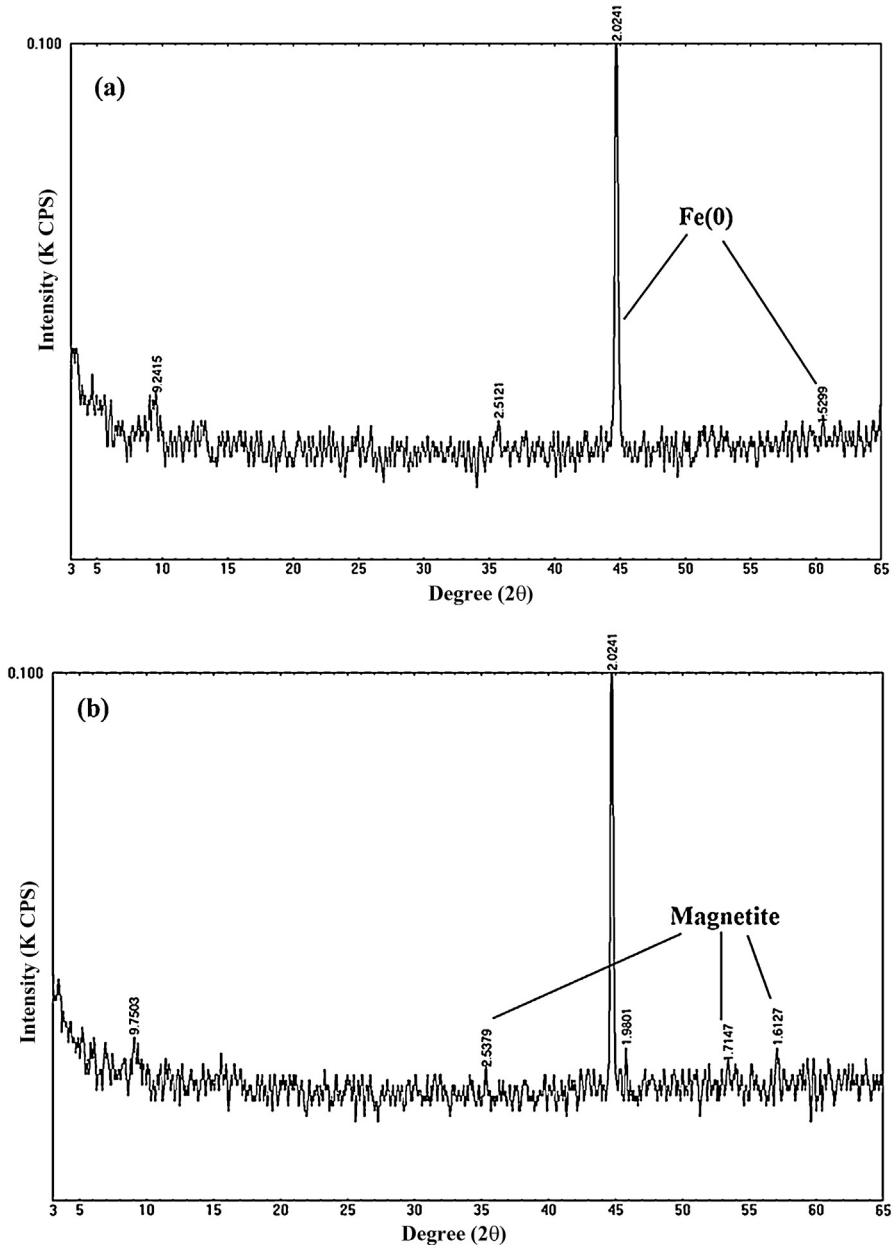


**Fig. 5 – X-ray diffraction spectra for (a) zero-valent iron (ZVI) and (b) acid-purged zero-valent iron (APZ).**

fitting data for magnetite provided by Montoro (1938) (Paulus and Vautier, 1980) were similar to the $d$ [Å], $2\theta$ [deg], and $I$ [%], which are 2.52787, 35.483, and 100.0, respectively, obtained in our analysis. Moreover, magnetite forms were completely absent in the XRD spectra of ZVI, probably because it was less than the detection limit (<1% by weight) (Diez-Perez et al., 2006). The percentage composition of Fe from the EDX and XRD analysis demonstrates that the APZ corrosion products are a mixture of amorphous $Fe_2O_3$, iron(III) oxide/hydroxide, magnetite ($Fe_3O_4$), and/or maghemite ($\gamma$-$Fe_2O_3$), and lepidocrocite ($\gamma$-FeOOH), indicating that Fe(II) formation is not an intermediate step in the APZ corrosion process (Kanel et al., 2005). Though the signal intensities obtained for APZ in the XRD analysis were weak, few elevated baseline peaks at $2\theta = 30$ and $2\theta = 53$ correspond to lepidocrocite ($\gamma$-FeOOH). In the EDX analysis, the APZ surface corrosion product ratio Fe:O:As = 50:17:1 respectively. The most likely solid phases hosting sorbed As(V) and As(III) in the APZ system are iron oxides and magnetite (as confirmed by XRD analysis), which are products of thermodynamic processes, with the later possessing greater stability under anaerobic conditions (Odziemkowski et al., 1998). Lesser kinetic processes may produce other strong precipitates and formation of inner-sphere complexes of As(V) and As(III) on ferrihydrite as reported by Su and Puls (2004).

### 3.2. *Effects of operating conditions on DCMD flux*

#### 3.2.1. *Influence of As-feed temperature on distillate flux*

Within a temperature range of 50–80 °C, the amount of flux generated using PTFE0221, PTFE0221B and MSPP270045 membrane was studied as shown in Fig. 6. During the experiment, we observed that distillate flux increases with the increase of feed side temperature. The vapor pressures at the liquid–vapor boundary exponentially increase with temperature increase as computed using Antoine Eq. (2). In addition, an increase in feed temperature reduces the resistance imposed by the heat and mass transfer interface, allowing the more viscous fluid to escape through the membrane. Results from this study concur with findings reported by Hou et al. (2010).

At a constant feed and distillate flow rate of 0.78 and 0.86 L/min, increase in temperature from 50 °C to 80 °C produced a corresponding increase in distillate/water flux rate from 26.7 to 55.5 kg/m$^2$ h for PTFE0221, 22.4 to 51.8 kg/m$^2$ h for PTFE0221B and 19.8 to 45.7 kg/m$^2$ h for MSPP270045. In all the three membranes, an exponential increase in flux was found confirming that increase in vapor pressure is proportional to increase in temperature as shown in Eq. (2). At high temperatures, the thermal efficiency of the system has a more pronounced effect on the amount of heat transfer by conduction than that transmitted by the diffusing species. Also, a higher flux was observed using PTFE than in PP membranes. This may be due to increased porosity of PTFE0221(B) membranes and its high hydrophobicity, the mode of fabrication and uniform surfaces (especially that of the supporting layer) of PTFE membranes which aids the assimilation of gaseous species at the membrane interface. Supporting substrate of the composite membranes of PTFE also plays a role in the amount of flux generated. The polypropylene substrate layer enhanced assimilation of the diffusing species due to blending of the pore structures with the PTFE active layer than does the polyethylene terephthalate support layer (Fig. 6).

#### 3.2.2. *Influence of feed concentration on distillate flux*

Distillate arsenic concentration as a function of increasing feed concentration was studied by setting feed and distillate inlet velocity at 0.85 and 1.30 L/min, respectively, with varying arsenic concentrations of 0.05–1.4 mg/l. Noticeable decline in the amount of distillate flux for the three membranes was observed as shown in Fig. 7. However, in MSPP270045 (PP/PET) membrane, a linear relationship between the amount of distillate flux and feed concentration tends to emerge at a temperature range of 60–70 °C. About 15.2% flux decline was observed in PTFE0221, 16.6% in PTFE0221B and 10.5% in MSPP270045. The result obtained in this study is similar to that observed in a study by Pal and Manna (2010), where the influence of wide range arsenic concentrations (0–1.2 mg/l) on distillate flux was considered insignificant. However, this was not the case in another study conducted by Khayet et al. (2004), where the MD configuration displayed wide declines in flux production as salt concentration was raised from 600 to 120,000 mg/l. This decline is often associated with the reduction in water activity caused by increase in concentration of arsenic feed solution which constitutes a systemic barrier for water vapor evaporation at the feed-membrane boundary.

To counter this effect, we increase the feed flow rate in order to improve the water activity (see Section 3.2.3), this results in a noticeable increase of flux production from 3%

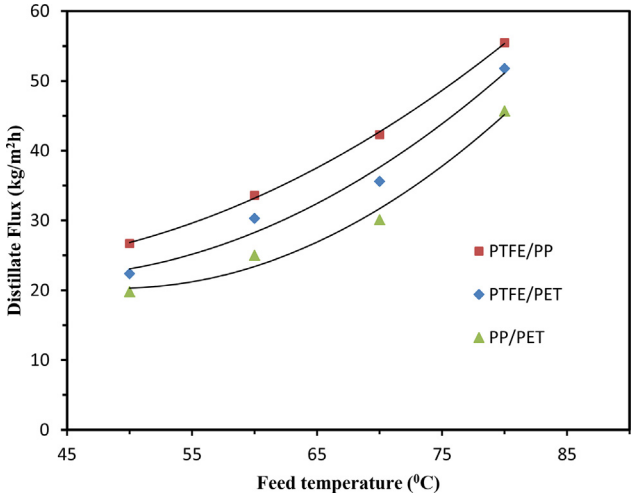


**Fig. 6 – Influence of feed temperature on distillate flux (at total As-feed concentration of 0.5 mg/l).**

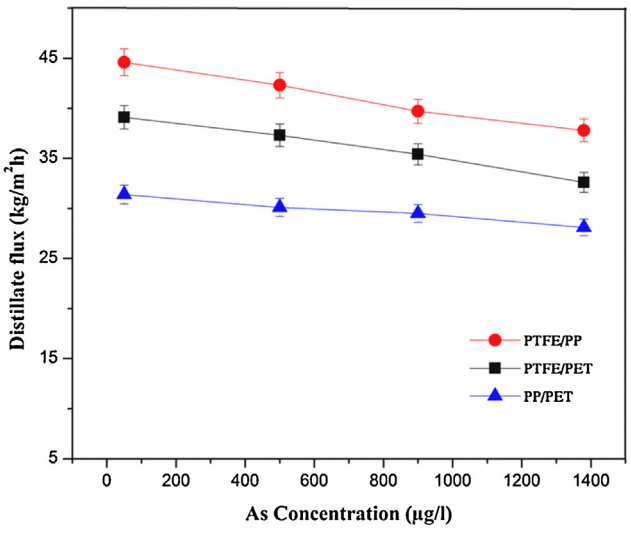


**Fig. 7 – Effect of total arsenic feed concentration on distillate flux (feed inlet temperature 60–70 °C).**

to 5% but this enhancement was not prominent in the overall flux production process. However, optimizing the hydrophobic properties of the membrane can ensure permeate production within the limit of portable water standard (Ozaki et al., 2002). In a recent study, it was observed that an increase of feed concentration in an RO process resulted in significant reduction of the process efficiency occasioned by decrease in mass transfer across the membrane (Kotb et al., 2015). These results suggest that concentration polarization remains a challenge using currently available membranes though, this effect have minimal effect on the amount of flux produced in MD processes.

### 3.2.3. *Effects of feed velocity on distillate flux*

To estimate the effect of feed flow rate/velocity on the amount of distillate produced, the feed and distillate streams were kept between 70 °C and 45 °C respectively. As described earlier, flux is directly related to fluid dynamics between the hot and cold streams (see Section 2.6). This effect for the three membranes; PTFE0221, PTFE0221B and MSPP270045, is presented in Fig. 8 where the feed flow rate was varied from 0.76 to 1.30 L/min. Results revealed that distillate flux improved with increase of feed flow rate. This is caused by decrease in boundary layer thickness and increase in coefficient of mass and heat transfer stemming from increased energetic feed flows. Therefore, following Eq. (1), temperature at the membrane interface ($T_{mh}$) is increased owing to the decrease of temperature polarization on the feed side and consequently generating higher mass transfer across the membrane.

Though increased fluid dynamics thins off the concentration boundary layer and thus, allowing the yield of higher distillate flux, the effect of temperature polarization is readily seen on distillate flux than concentration polarization. In addition, PTFE0221(B) membranes displayed better performance characteristics over MSPP270045 membrane, with the former having a higher flux values at the same feed flow rate. When the feed velocity was set at 1.3 L/min, the distillate flux nearly stabilized. This implies that a further increase in feed velocity might not yield a corresponding increase in distillate flux and hence proposing the optimum condition for feed velocity in the DCMD process.

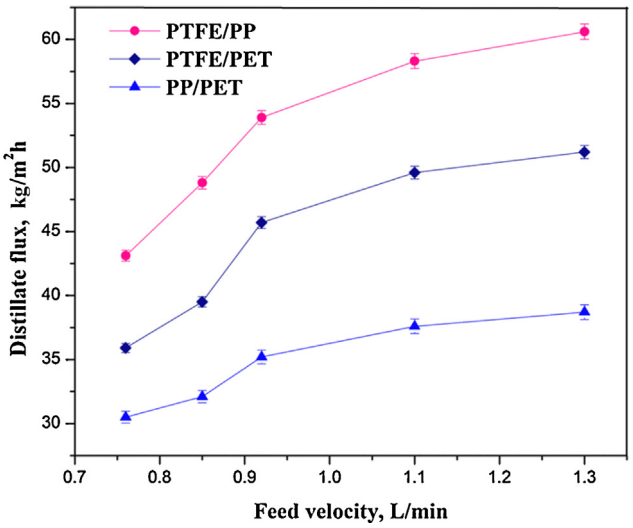


**Fig. 8 – Variation of feed velocity and distillate flux (total arsenic feed concentration = 0.5 mg/l).**

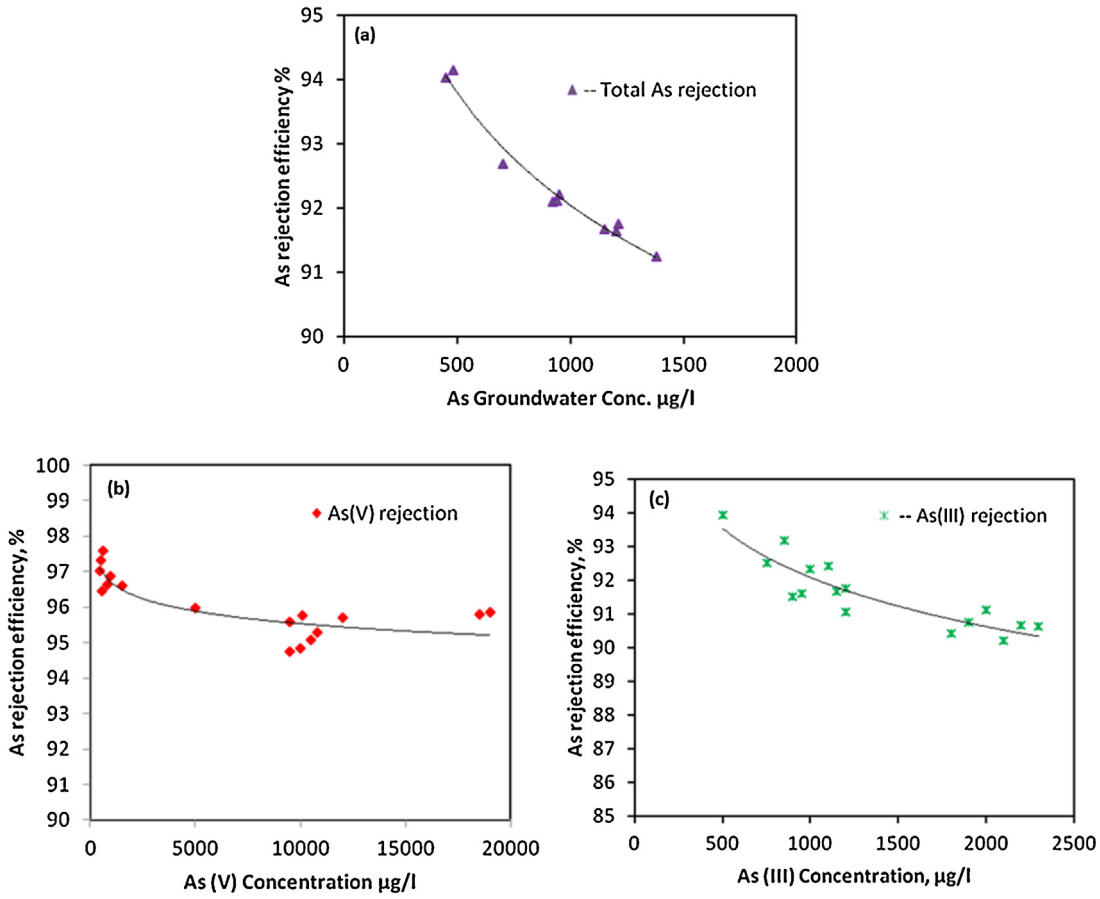


**Fig. 9 – Arsenic rejection efficiency as a function of: (a) varying total As concentration obtained from groundwater in Datong Basin and (b) different concentrations of simulated As(V) and (c) As(III) species.**

### 3.3. Arsenic removal system

#### 3.3.1. Arsenic rejection in DCMD process

As described in Eq. (3), the arsenic removal efficiency of the DCMD process using arsenic contaminated groundwater from Datong Basin in China and simulated solutions of arsenate and arsenite was estimated (Fig. 9). As the concentration of arsenic increases, a corresponding decrease in arsenic removal efficiency was observed. This could be as a result of membrane wetting – a common characteristic observed in variety of membranes after long hours of operation, occasioned by slight changes in morphology and pore sizes of the three membranes utilized in this study.

In all the experiments, arsenic removal efficiency was greater than 90% and in some cases, nearly 99% removal was achieved at an initial concentration of 100 μg/l. As(V) removal rate was higher compared to As(III) as shown in (Fig. 9b and c). This phenomenon was also found in pressure-driven processes (Sato et al., 2002; Xia et al., 2007), highlighting the importance of contaminant charge properties in pressure-driven process. However, it is expected that both inorganic forms of arsenic should be rejected in the DCMD process because the membranes used are hydrophobic. But this was not the case, as there were micro-fractions of As(III) found in permeate more than As(V). It is known that As(III) exists in neutral state at pH 6.5 ± 1.5, while As(V) occurs in a negatively charge monovalent state at pH above 4 (Kang et al., 2000). However, at high As concentrations, negatively charge conditions are temporarily induced on the surface of the hydrophobic membranes in solution making it slightly hydrophilic. This creates a stronger electrostatic repulsion of arsenate, retaining it on the feed side (though a weak charge may not be enough to cause ions to be retained) but exhibited less effect on As(III) due to charge exclusion under the given pH condition. Unlike pressure driven processes, the MD technique proves advantageous because it involves very low pressure operation utilizing mass transfer of water vapor particles through electrostatic membranes with less effect related to charge of contaminants.

#### 3.3.2. Arsenic immobilization and reduction by APZ

Fig. 10 shows the removal of As(V) using 2 g acid-purged ZVI (APZ) at pH 7. The amounts of arsenic removed were attributed to the association of arsenic with APZ because they were not suspended in the solutions. Results obtained from the analysis clearly show that APZ is capable of immobilizing As(V) with reasonably fast kinetics and reduction to elemental arsenic is also a feasible mechanistic step. Conditions determining final arsenic speciation after reaction with APZ include: arsenic concentration, solution pH, and the properties of zero valent iron (ZVI) materials. Under conditions of low As(V) concentration, the ratio of dissolved As(V) to uncomplexed ZVI corrosion products (i.e. oxyhydroxides) is sufficiently low that there is no competition between As(V) species for complexation sites. This situation results in removal kinetics that are first order in As(V) concentration as described in Section 3.4.

On the other hand, increase in As(V) concentration elevates the ratio of aqueous arsenate to available complexation sites, creating competition within the sites. This results in reduced As(V) removal rate due to subsequent aging of ZVI corrosion products (Farrell et al., 2001). Physical structures of ZVI/$Fe^0$ and APZ explain the reason for their different reactivities. ZVI surface is covered by iron oxide films in water and consequently inhibits reaction of As(V) with the ZVI core. This may be due to co-precipitation of arsenic with iron corrosion

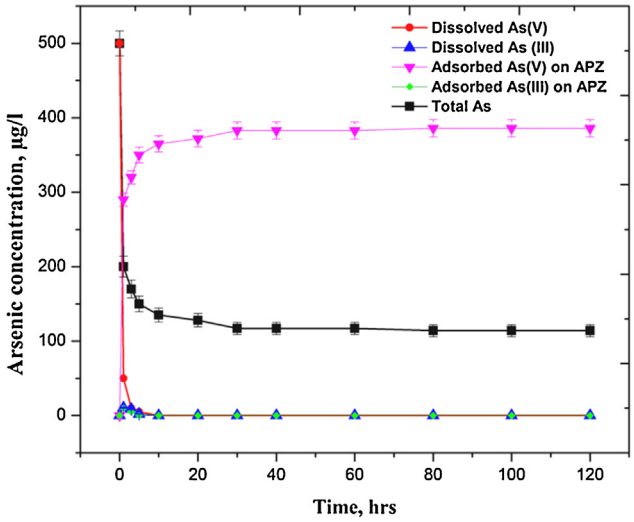


**Fig. 10 – Adsorption and reduction experiment of As(V) to As(0) using less than 2 g acid-purged ZVI (APZ) under strict anoxic condition at pH 7 (total As(V) = 0.50 mg/l in separate solutions).**

product. At this stage, the iron oxide film formed is less porous or the kinetics of iron corrosion is lower which could make the reduction/removal process less quantitative (Noubactep, 2008). However, it has been reported that after aging of iron oxides, subsequent production of other iron corrosion products like carbonate green rust (which are eventually converted to magnetite under anaerobic conditions) will continue to function to degrade and immobilize contaminants even after the exhaustion of the elemental iron (Su and Puls, 2004). Here, adsorption plays a major role for As(V) immobilization. However, the further transformation to magnetite can induce the reduction of arsenic after being adsorbed as described in the reaction below:

$$Fe \rightarrow Fe^{2+} + 2e, \quad Fe^{2+} \rightarrow Fe^{3+} + e;$$

$$As^{5+} + 2e \rightarrow As^{3+}, \quad As^{3+} + 3e \rightarrow As^{0}$$

In the same vein, other investigators have described the reaction of nanoscale ZVI (5 g/l) with arsenic for up to 15 days at 100 mg/l As(V) concentration, and the results indicate that no significant change in arsenic distributions or speciation was detected compared to samples reacted for 24 h under similar conditions (Ramos et al., 2009).

Purging ZVI with acid (APZ) enables the breakdown of the pervasive iron oxide film, producing a highly porous and oxidized iron structure. This reactive material (APZ) produced, promoted reaction between the matrix enmeshed contaminants and the iron core during the arsenic reduction process. Some authors have shown that since As(V) is readily reduced to As(0) by iron in acidic media. This infers that several pH-dependent factors may be responsible for the As reduction process (Farrell et al., 2001; Bang et al., 2005; Ramos et al., 2009). At low pH, the non-porous oxide barrier hindering As(V) access to the iron core phase is basically reduced. Although iron oxides cover the iron core at neutral pH values, the oxides are minimally porous, and partially protect the underlying core from attack by oxidants in solution (Farrell et al., 2001). Therefore, aqueous arsenate/arsenite would still have some access to the iron core in neutral media. Here, the advantage of the DCMD-APZ process plays out in the ability to adjust the system pH at the second phase treatment with APZ to immobilize

or reduce high concentration of residual arsenic (as demonstrated using spectroscopic analysis) generated after DCMD run. In this way, secondary contamination of the groundwater environment could be prevented and elemental arsenic (As[0]) produced can be put to other use.

### 3.3.3. *Spectroscopic analysis*

Reduction of As(V) to As(III) and As(0) using APZ was confirmed by high resolution As 3d XPS spectra analysis (Fig. 11). Various forms of arsenic species have characteristics binding energies (BEs) relating to their respective 3d-sub-orbital photoelectron. Shifts in As 3d BEs occur in different arsenic species. For instance, $AsO_4^{3-}$ has a BE of 44.9 eV, $HAsO_4^{2-}$ has BE = 45.5 eV, and $H_2AsO_4^-$ has BE = 46.7 eV (Wagner et al., 1979). Other investigators reported that As(V) in $Na_2HAsO_4$ has a 3d BE of 45.5 eV, while As(III) and As(0) have BEs of 44.2 and 41.5 respectively (Roberts et al., 1975). In the reaction of ≤2 g APZ with residual As concentration of 10 mg/l, the XPS spectra exhibited three prominent peaks at 45.45 eV, 44.1 eV and 41.4 eV associated with As 3d peaks of As(V), As(III) and As(0) respectively. The As(V) reduction experiment as observed from the XPS peak analysis at different pH values are shown in Table 3. However, the partial reduction to As(III) observed here and by other authors may be due to the highly negative surface potential of reacting species (greater than −150 mV) which can cause a decrease in the equilibrium potential of As(V)/As(0) redox couple, making As(V) reduction to elemental arsenic less favorable (Farrell et al., 2001). However, the detection of As(0) on APZ surface supports the evidence that As(V) is reduced to metallic As(0) under strict anoxic conditions (Sun et al., 2011). $Cu^{2+}$, $Hg^{2+}$ and other metals have been reduced to their zero-valence states using nanoparticles of ZVI (O'Carroll et al., 2013). In this vein, nanoparticles of ZVI and APZ could be said to possess similar reactivity and could by their chemistry and structure open up a contact for As contaminant species to reach the Fe(0) core.

Effects of pH condition on arsenic reduction/adsorption were evaluated. At pH 7, arsenic adsorption capacity on APZ was very fast (see Section 3.4); however, the reduction capacity was low at this pH value when compared to the As(0) peaks of As 3d binding energies at pH 5 and 6 (Fig. 11b). This observation suggests that at pH 7, adsorption of As(V) onto APZ was the dominant reaction. However, reduction of arsenate to arsenite and metallic arsenic was more dominant at pH less than 7, under rigorous anoxic conditions. Some researchers described the slow reduction of arsenate ranging from 2 to 3 months lag time (Bang et al., 2005). This may be as a result of the presence of dissolved oxygen in their experimental procedures which may inhibit the reduction kinetics. Previous report revealed that arsenite could be oxidized to arsenate on reaction with iron oxides complexes in the presence of oxygen (Hug and Leupin, 2003). The long ripening period observed by these researchers was probably an indication of the time needed for the complete exclusion of dissolved oxygen from the system. Hence, we ensure to conduct the experiment under strict anoxic atmosphere in the APZ reactors and thus, obtaining relatively faster arsenate reduction dynamics.

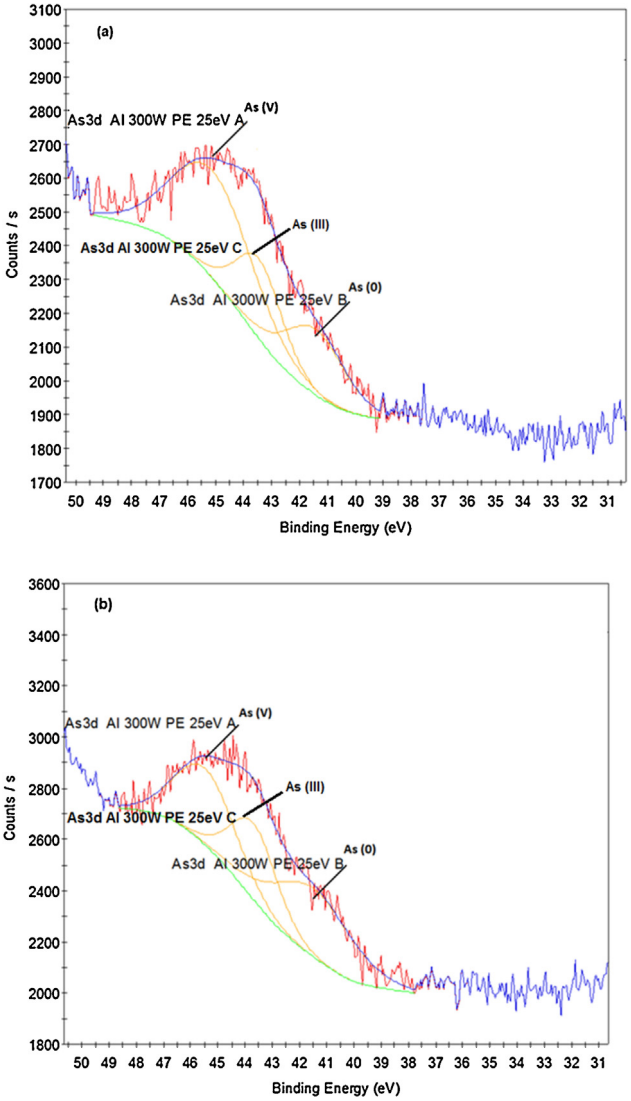


**Fig. 11 – XPS spectra at As 3d photoelectron Al Kα1.2 source type of As(V) reaction with APZ at (a) pH 7 and (b) pH 5, after 5 days under strict anoxic conditions (As(V) conc. = 10 mg/l at 30 °C).**

**Table 3 – Peak analysis of APZ reaction with As(V) and As(III) after 5 days.**

| Peak analysis | pH | BE (eV) | As species detected | As area ratio (%) |
|---|---|---|---|---|
| As3d Al 300 W PE 25 eV A | 5.0 | 45.45 | As(V) | 34.0 |
| As3d Al 300 W PE 25 eV B | | 41.49 | As(0) | 39.5 |
| As3d Al 300 W PE 25 eV C | | 43.7 | As(III) | 26.5 |
| As3d Al 300 W PE 25 eV A | 6.0 | 45.1 | As(V) | 53.2 |
| As3d Al 300 W PE 25 eV B | | 41.45 | As(0) | 23.9 |
| As3d Al 300 W PE 25 eV C | | 43.44 | As(III) | 22.9 |
| As3d Al 300 W PE 25 eV A | 7.0 | 45.29 | As(V) | 57.8 |
| As3d Al 300 W PE 25 eV B | | 41.04 | As(0) | 17.9 |
| As3d Al 300 W PE 25 eV C | | 43.23 | As(III) | 24.3 |

**Table 4 – Pseudo-first-order and second-order model and correlation coefficient for As removal on APZ.**

| pH | Arsenic species | Pseudo first-order model | | | $R^2$ | Pseudo second-order model | | | $R^2$ |
|---|---|---|---|---|---|---|---|---|---|
| | | $K_1$ ($h^{-1}$) | $q_e$ (mg/g) | $t_{1/2}$ (h) | | $K_2$ (g/mg h) | $q_e$ (mg/g) | $t_{1/2}$ (h) | |
| 7 | As(V) | 1.3638 | 370.27 | 0.513 | 0.945 | 0.0061 | 382.74 | – | 0.982 |
| | As (III) | 45.079 | 1.3636 | 0.006 | – | 4.67E45 | 1.3636 | – | – |

(–) Data unavailable.

### 3.4. *Adsorption kinetics models for arsenic removal*

To further investigate the adsorption mechanism of APZ, sorption kinetic models were used to explain the reaction rate and the time to reach equilibrium. The rate of As(V) adsorption was very fast at $t_{1/2}$ of approximately 30 min, adopting the non-linear pseudo first-order reaction kinetics. The apparent first-order kinetics reflected the rate of complex formation and the diffusional mass transfer limitations within the formed iron oxide phase on APZ, as suggested by other authors (Fuller et al., 1993). Both pseudo-first- and second-order model were investigated to estimate the sorption rate and the possible reaction mechanism. The pseudo-first-order kinetic model proposed by Lagergren (1898) was used (assuming non-dissociating molecular adsorption onto APZ) and it is represented as:

$$\ln(q_e - q_t) = \ln q_e - k_1 t \quad (5)$$

where $q_t$ is the amount of arsenic removed at time, $t$ (mg/g), $q_e$ is the adsorption capacity at equilibrium (mg/g), $k_1$ is the pseudo-first-order rate constant ($h^{-1}$), and $t$ is the contact time (h). The pseudo-second-order sorption kinetics is based on the assumption of chemisorption of arsenic on the APZ materials and is expressed as:

$$\frac{t}{q} = \frac{1}{k_2 \cdot q_e^2} + \frac{1}{q_e} t \quad (6)$$

where $K_2$ is the rate of sorption (g/mg h) for the second-order reaction, $q_e$ the amount of arsenic adsorbed onto APZ at equilibrium (mg/g) and $q$ is the quantity of arsenic adsorbed at any time (mg/g).

The pseudo-first-order ($k_1$) and second-order ($k_2$) rate constants determined from the kinetic model are presented in Table 4, describing the removal of total arsenic by APZ at 30 °C. In all the reactions, dissolved arsenic concentration reduced exponentially with time till equilibrium conditions are reached. As expected, the amount of adsorbed arsenic increased with increasing equilibrium concentration of aqueous arsenic. Adsorbed As(III) did not fit well using the pseudo-first-order and second-order models. This may be due to very low content of As(III), or because of the relative weak affinity of As(III) for APZ surface at neutral pH. The concentration of arsenate declined with time, though the arsenic analytical procedures revealed that aggregation of arsenite was almost absent. Thus, an assumption that arsenate was reduced to elemental arsenic in a thermodynamically aided system of DCMD-APZ is feasible.

Similar observations were made by Pourbaix (1966) and Sun et al. (2011), where they demonstrated that Fe(0) can reduce As(V) to As(0) using acid-treated zero-valent iron, and partially reduced As(V) to As(III) and metallic arsenic respectively. Moreover, the more selective electron conduction of APZ surface layer such as the magnetite layer (Xu et al., 2012) allows the transfer of electrons from the electron rich ZVI core to residual As(V) or As(III) at the particle surface, hence achieving efficient contaminant immobilization. The half-life of a pseudo-second-order reaction is negligible since it depends on the initial concentration in contrast to its constancy for a pseudo-first-order reaction. The $R^2$ values obtained from kinetic models for As(V) immobilized by APZ show that the pseudo-second-order model fitted better than the pseudo-first-order model. This indicates that chemisorption dominated the adsorption process. However, predictable values for half-life determination for this model were unavailable, supporting the concept that half-life for a pseudo-second-order reaction is far less useful. Other adsorption models like Weber and Morris intra-particle diffusion model and Boyd kinetic model were not used as this work solely focuses on explaining the transformational role of APZ on residual arsenic ions immobilization and reduction by the DCMD-APZ configuration. However, further study should be conducted to understand the rate limiting steps and interaction mechanism of arsenic ions at the surface and the interior portions of APZ.

## 4. Conclusions

In this present study, we have clearly demonstrated the robustness of combined treatment process for decontamination of high arsenic groundwater and immobilization of residual arsenic by the integration of direct contact membrane distillation with acid-purged zero-valent ion (DCMD-APZ). The DCMD-APZ configuration showed excellent capacity for high arsenic removal up to 20 mg/l with a maximum arsenic rejection efficiency greater than 90%, and nearly 99% removal achieved at an initial concentration of 100 μg/l. Among the membranes used, PTFE0221 was the most efficient for arsenic removal when compared to other membrane utilized in the study (PTFE0221B and MSPP270045). At a constant feed and distillate flow rate of 0.78 and 0.86 L/min, increase in temperature from 50 °C to 80 °C produced a corresponding increase in distillate/water flux rate from 26.7 to 55.5 kg/$m^2$ h for PTFE0221, 22.4 to 51.8 kg/$m^2$ h for PTFE0221B and 19.8 to 45.7 kg/$m^2$ h for MSPP270045. Also, it was observed that both species of inorganic arsenic (As[V] and As[III]) can be effectively sequestered under anaerobic conditions without the possibility of secondary release since contaminants enmeshed in iron corrosion products of APZ are stable under environmental conditions. XPS spectra of As-APZ surface at slightly acidic pH and high As-concentration showed increased presence of As(0). This observation led to the conclusion that hybrid configuration of the DCMD-APZ technique can be a more efficient technology for removal and reduction/immobilization of high concentrations of arsenic generated in a system which is thermodynamically assisted.

Further, the operation of the DCMD-APZ technology requires limited maintenance and when a suitable membrane is selected, such as the PTFE/PP type, this could result in generation of higher flux at a low cost of operation.

## Acknowledgements

This work was financially supported by National High Technology Research and Development, Program, China on "Natural low-quality groundwater remediation and demonstration" (no. 2012AA062602). Abass O.K. wishes to thank the China Scholarship Council (CSC) for the scholarship support. The authors thank Dr. Dingguo Tang, for helping with the interpretation of the XPS data.

## References

Aleksanyan, A.Y., Podobaev, A.N., Reformatskaya, I.I., 2007. Steady-state anodic dissolution of iron in neutral and close-to-neutral media. Prot. Met. 43 (1), 66–69, http://dx.doi.org/10.1134/s003317320701009.

Alowitz, M.J., Scherer, M.M., 2002. Kinetics of nitrate, nitrite, and Cr(VI) reduction by iron metal. Environ. Sci. Technol. 36 (3), 299–306, http://dx.doi.org/10.1021/es011000h.

Baikousi, M., Georgiou, Y., Daikopoulos, C., Bourlinos, A.B., Filip, J., Zbořil, R., et al., 2015. Synthesis and characterization of robust zero valent iron/mesoporous carbon composites and their applications in arsenic removal. Carbon 93, 636–647, http://dx.doi.org/10.1016/j.carbon.2015.05.081.

Balakumar, P., Kaur, J., 2009. Arsenic exposure and cardiovascular disorders: an overview. Cardiovasc. Toxicol. 9 (4), 169–176, http://dx.doi.org/10.1007/s12012-009-9050-6.

Bang, S., Johnson, M.D., Korfiatis, G.P., Meng, X.G., 2005. Chemical reactions between arsenic and zero-valent iron in water. Water Res. 39 (5), 763–770, http://dx.doi.org/10.1016/j.watres.2004.12.022.

Barbe, A.M., Hogan, P.A., Johnson, R.A., 2000. Surface morphology changes during initial usage of hydrophobic, microporous polypropylene membranes. J. Membr. Sci. 172 (1–2), 149–156, http://dx.doi.org/10.1016/S0376-7388(00)00338-0.

Bomben, K.D., Moulder, J.F., Sobol, P.E., Stickle, W.F., 1995. Handbook of X-ray Photoelectron Spectroscopy. A Reference Book of Standard Spectra for Identification and Interpretation of XPS Data. Physical Electronics, Eden Prairie, MN.

Deng, H.H., Nanjo, H., Qian, P., Xia, Z.B., Ishikawa, I., 2006. Evolution of passivity in air exposure of an iron passive film. Electrochim. Acta 52 (1), 187–193, http://dx.doi.org/10.1016/j.electacta.2006.04.057.

Diez-Perez, I., Sanz, F., Gorostiza, P., 2006. In situ studies of metal passive films. Curr. Opin. Solid State Mater. Sci. 10 (3–4), 144–152, http://dx.doi.org/10.1016/j.cossms.2007.01.002.

Farrell, J., Wang, J., O'Day, P., Conklin, M., 2001. Electrochemical and spectroscopic study of arsenate removal from water using zero-valent iron media. Environ. Sci. Technol. 35 (10), 2026–2032, http://dx.doi.org/10.1021/es0016710.

Fuller, C.C., Davis, J.A., Waychunas, G.A., 1993. Surface chemistry of ferrihydrite: Part 2: Kinetics of arsenate adsorption and coprecipitation. Geochim. Cosmochim. Acta 57 (10), 2271–2282, http://dx.doi.org/10.1016/0016-7037(93)90568-h.

Hou, D.Y., Wang, J., Sun, X.C., Luan, Z.K., Zhao, C.W., Ren, X.J., 2010. Boron removal from aqueous solution by direct contact membrane distillation. J. Hazard. Mater. 177 (1–3), 613–619, http://dx.doi.org/10.1016/j.jhazmat.2009.12.076.

Huang, F.G., Jia, S.Y., Liu, Y., Wu, S.H., Han, X., 2015. Reductive dissolution of ferrihydrite with the release of As(V) in the presence of dissolved S(-II). J. Hazard. Mater. 286, 291–297, http://dx.doi.org/10.1016/j.jhazmat.2014.12.035.

Hug, S.J., Leupin, O., 2003. Iron-catalyzed oxidation of arsenic(III) by oxygen and by hydrogen peroxide: pH-dependent formation of oxidants in the Fenton reaction. Environ. Sci. Technol. 37 (12), 2734–2742, http://dx.doi.org/10.1021/Es026208x.

Jadhav, S.V., Bringas, E., Yadav, G.D., Rathod, V.K., Ortiz, I., Marathe, K.V., 2015. Arsenic and fluoride contaminated groundwaters: a review of current technologies for contaminants removal. J. Environ. Manage. 162, 306–325, http://dx.doi.org/10.1016/j.jenvman.2015.07.020 (review).

Kanel, S.R., Manning, B., Charlet, L., Choi, H., 2005. Removal of arsenic(III) from groundwater by nanoscale zero-valent iron. Environ. Sci. Technol. 39 (5), 1291–1298, http://dx.doi.org/10.1021/Es048991u.

Kang, M., Kawasaki, M., Tamada, S., Kamei, T., Magara, Y., 2000. Effect of pH on the removal of arsenic and antimony using reverse osmosis membranes. Desalination 131 (1–3), 293–298, http://dx.doi.org/10.1016/S0011-9164(00)90027-4.

Khayet, M., Godino, M.P., Mengual, J.I., 2004. Study of asymmetric polarization in direct contact membrane distillation. Sep. Sci. Technol. 39 (1), 125–147, http://dx.doi.org/10.1081/Ss-120027405.

Kong, S., Wang, Y., Hu, Q., Abass, O.K., 2014. Magnetic nanoscale Fe–Mn binary oxides loaded zeolite for arsenic removal from synthetic groundwater. Coll. Surf. A: Physicochem. Eng. Aspects 457, 220–227, http://dx.doi.org/10.1016/j.colsurfa.2014.05.066.

Kotb, H., Amer, E.H., Ibrahim, K.A., 2015. Effect of operating conditions on salt concentration at the wall of RO membrane. Desalination 357, 246–258, http://dx.doi.org/10.1016/j.desal.2014.12.002.

Lackovic, J.A., Nikolaidis, N.P., Dobbs, G.M., 2000. Inorganic arsenic removal by zero-valent iron. Environ. Eng. Sci. 17 (1), 29–39, http://dx.doi.org/10.1089/ees.2000.17.29.

Lagergren, S., 1898. Zur theorie der sogenannten adsorption gelöster stoffe. Kungliga Svenska Vetenskapsakademiens. Handlingar 4 (Band 24), 1–39 (journal).

Lai, K.C.K., Lo, I.M.C., 2008. Removal of chromium(VI) by acid-washed zero-valent iron under various groundwater geochemistry conditions. Environ. Sci. Technol. 42 (4), 1238–1244, http://dx.doi.org/10.1021/es071572n.

Li, J., Shi, Z., Ma, B., Zhang, P., Jiang, X., Xiao, Z., et al., 2015. Improving the reactivity of zerovalent iron by taking advantage of its magnetic memory: implications for arsenite removal. Environ. Sci. Technol. 49 (17), 10581–10588, http://dx.doi.org/10.1021/acs.est.5b02699.

Mak, M.S., Rao, P., Lo, I.M., 2009. Effects of hardness and alkalinity on the removal of arsenic(V) from humic acid-deficient and humic acid-rich groundwater by zero-valent iron. Water Res. 43 (17), 4296–4304, http://dx.doi.org/10.1016/j.watres.2009.06.022.

Martinez-Diez, L., Vazquez-Gonzalez, M.I., 1999. Temperature and concentration polarization in membrane distillation of aqueous salt solutions. J. Membr. Sci. 156 (2), 265–273, http://dx.doi.org/10.1016/S0376-7388(98)00349-4.

Mayo, J.T., Yavuz, C., Yean, S., Cong, L., Shipley, H., Yu, W., et al., 2007. The effect of nanocrystalline magnetite size on arsenic removal. Sci. Technol. Adv. Mater. 8 (1–2), 71–75, http://dx.doi.org/10.1016/j.stam.2006.10.005.

Mazumder, D.N.G., Haque, R., Ghosh, N., De, B.K., Santra, A., Chakraborty, D., et al., 1998. Arsenic levels in drinking water and the prevalence of skin lesions in West Bengal, India. Int. J. Epidemiol. 27 (5), 871–877.

Mielczarski, J.A., Atenas, G.M., Mielczarski, E., 2005. Role of iron surface oxidation layers in decomposition of azo-dye water pollutants in weak acidic solutions. Appl. Catal. B: Environ. 56 (4), 289–303, http://dx.doi.org/10.1016/j.apcatb.2004.09.017.

Mukherjee, S.C., Rahman, M.M., Chowdhury, U.K., Sengupta, M.K., Lodh, D., Chanda, C.R., et al., 2003. Neuropathy in arsenic toxicity from groundwater arsenic contamination in West Bengal, India. J. Environ. Sci. Health A: Tox. Hazard. Subst. Environ. Eng. 38 (1), 165–183.

Navas-Acien, A., Silbergeld, E.K., Pastor-Barriuso, R., Guallar, E., 2008. Arsenic exposure and prevalence of type 2 diabetes in US adults. J. Am. Med. Assoc. (JAMA) 300 (7), 814–822, http://dx.doi.org/10.1001/jama.300.7.814.

Noubactep, C., 2006. Contaminant reduction at the surface of elemental iron: the end of a myth. Wissenschaftliche Mitteilungen 31, 173–179.
Noubactep, C., 2008. A critical review on the process of contaminant removal in $Fe^0$-$H_2O$ systems. Environ. Technol. 29 (8), 909–920, http://dx.doi.org/10.1080/09593330802131602.
O'Carroll, D., Sleep, B., Krol, M., Boparai, H., Kocur, C., 2013. Nanoscale zero valent iron and bimetallic particles for contaminated site remediation. Adv. Water Resour. 51, 104–122, http://dx.doi.org/10.1016/j.advwatres.2012.02.005.
Odziemkowski, M.S., Schuhmacher, T.T., Gillham, R.W., Reardon, E.J., 1998. Mechanism of oxide film formation on iron in simulating groundwater solutions: Raman spectroscopic studies. Corros. Sci. 40 (2–3), 371–389, http://dx.doi.org/10.1016/s0010-938x(97)00141-8.
Ozaki, H., Sharma, K., Saktaywin, W., 2002. Performance of an ultra-low-pressure reverse osmosis membrane (ULPROM) for separating heavy metal: effects of interference parameters. Desalination 144 (1–3), 287–294, http://dx.doi.org/10.1016/S0011-9164(02)00329-6.
Pal, P., Manna, A.K., 2010. Removal of arsenic from contaminated groundwater by solar-driven membrane distillation using three different commercial membranes. Water Res. 44 (19), 5750–5760, http://dx.doi.org/10.1016/j.watres.2010.05.031.
Paulus, M., Vautier, R., 1980. 4.1.3.11 References for 4.1.3 12b, 158–160, http://dx.doi.org/10.1007/10201640_56.
Pourbaix, M., 1966. Atlas of Electrochemical Equilibria in Aqueous Solutions. Pergamon Press, Oxford.
Qu, D., Wang, J., Hou, D.Y., Luan, Z.K., Fan, B., Zhao, C.W., 2009. Experimental study of arsenic removal by direct contact membrane distillation. J. Hazard. Mater. 163 (2–3), 874–879, http://dx.doi.org/10.1016/j.jhazmat.2008.07.042.
Ramos, M.A.V., Yan, W., Li, X.-q., Koel, B.E., Zhang, W.-x., 2009. Simultaneous oxidation and reduction of arsenic by zero-valent iron nanoparticles: understanding the significance of the core-shell structure. J. Phys. Chem. C 113 (33), 14591–14594, http://dx.doi.org/10.1021/jp9051837.
Roberts, E.D., Weightman, P., Johnson, C.E., 1975. Photoelectron and L2,3 MM Auger-electron energies for arsenic. J. Phys. C: Solid State Phys. 8 (8), 1301–1309, http://dx.doi.org/10.1088/0022-3719/8/8/032.
Sanchez-Rodas, D., Corns, W.T., Chen, B., Stockwell, P.B., 2010. Atomic fluorescence spectrometry: a suitable detection technique in speciation studies for arsenic, selenium, antimony and mercury. J. Anal. At. Spectr. 25 (7), 933–946, http://dx.doi.org/10.1039/B917755h.
Sato, Y., Kang, M., Kamei, T., Magara, Y., 2002. Performance of nanofiltration for arsenic removal. Water Res. 36 (13), 3371–3377, http://dx.doi.org/10.1016/S0043-1354(02)00037-4.
Schofield, R.W., Fane, A.G., Fell, C.J.D., 1990. Gas and vapor transport through microporous membranes. 2. Membrane distillation. J. Membr. Sci. 53 (1–2), 173–185, http://dx.doi.org/10.1016/0376-7388(90)80012-B.
Shannon, M.A., Bohn, P.W., Elimelech, M., Georgiadis, J.G., Marinas, B.J., Mayes, A.M., 2008. Science and technology for water purification in the coming decades. Nature 452 (7185), 301–310, http://dx.doi.org/10.1038/Nature06599.
Su, C., Puls, R.W., 2004. Significance of iron(II,III) hydroxycarbonate green rust in arsenic remediation using zerovalent iron in laboratory column tests. Environ. Sci. Technol. 38 (19), 5224–5231, http://dx.doi.org/10.1021/es0495462.
Sun, F.L., Osseo-Asare, K.A., Chen, Y.S., Dempsey, B.A., 2011. Reduction of As(V) to As(III) by commercial ZVI or As(0) with acid-treated ZVI. J. Hazard. Mater. 196, 311–317, http://dx.doi.org/10.1016/j.jhazmat.2011.09.029.
Triszcz, J.M., Porta, A., Einschlag, F.S.G., 2009. Effect of operating conditions on iron corrosion rates in zero-valent iron systems for arsenic removal. Chem. Eng. J. 150 (2–3), 431–439, http://dx.doi.org/10.1016/j.cej.2009.01.029.
Vadahanambi, S., Lee, S.H., Kim, W.J., Oh, I.K., 2013. Arsenic removal from contaminated water using three-dimensional graphene-carbon nanotube-iron oxide nanostructures. Environ. Sci. Technol. 47 (18), 10510–10517, http://dx.doi.org/10.1021/Es401389g.
Vahidnia, A., van der Voet, G.B., de Wolff, F.A., 2007. Arsenic neurotoxicity – a review. Hum. Exp. Toxicol. 26 (10), 823–832, http://dx.doi.org/10.1177/0960327107084539.
Wagner, C.D., Riggs, W.M., Davis, L.E., Moulder, J.F., Muilenberg, G.E., 1979. Handbook of X-Ray Photoelectron Spectroscopy. Perkin-Elmer Corporation, Physical Electronics Division, Eden Prairie, MN.
Wang, P., Chung, T.-S., 2015. Recent advances in membrane distillation processes: membrane development, configuration design and application exploring. J. Membr. Sci. 474, 39–56, http://dx.doi.org/10.1016/j.memsci.2014.09.016.
Wang, P., Chung, T.S., 2013. A new-generation asymmetric multi-bore hollow fiber membrane for sustainable water production via vacuum membrane distillation. Environ. Sci. Technol. 47 (12), 6272–6278, http://dx.doi.org/10.1021/es400356z.
Wang, P., Cui, Y., Ge, Q., Fern Tew, T., Chung, T.-S., 2015. Evaluation of hydroacid complex in the forward osmosis–membrane distillation (FO–MD) system for desalination. J. Membr. Sci. 494, 1–7, http://dx.doi.org/10.1016/j.memsci.2015.07.022.
Wang, S., Wu, X., Tan, M., Gong, J., Tan, W., Bian, B., et al., 2012. Fighting fire with fire: poisonous Chinese herbal medicine for cancer therapy. J. Ethnopharmacol. 140 (1), 33–45, http://dx.doi.org/10.1016/j.jep.2011.12.041.
Wichterle, I., Linek, J., 1971. Antoine Vapor Pressure Constants of Pure Compounds. Academia, Prague.
Xia, S.J., Dong, B.Z., Zhang, Q.L., Xu, B., Gao, N.Y., Causseranda, C., 2007. Study of arsenic removal by nanofiltration and its application in China. Desalination 204 (1–3), 374–379, http://dx.doi.org/10.1016/j.desal.2006.04.035.
Xie, K., Wang, X.-x., Liu, Z.-j., Alsaedi, A., Hayat, T., Wang, X.-k., 2014. Synthesis of flower-like $\alpha$-$Fe_2O_3$ and its application in wastewater treatment. J. Zhejiang Univ. Sci. A 15 (8), 671–680, http://dx.doi.org/10.1631/jzus.A1400133.
Xu, J., Hao, Z., Xie, C., Lv, X., Yang, Y., Xu, X., 2012. Promotion effect of $Fe^{2+}$ and $Fe_3O_4$ on nitrate reduction using zero-valent iron. Desalination 284, 9–13, http://dx.doi.org/10.1016/j.desal.2011.08.029.
Yadav, I.C., Devi, N.L., Singh, S., 2015. Reductive dissolution of iron-oxyhydroxides directs groundwater arsenic mobilization in the upstream of Ganges River basin, Nepal. J. Geochem. Explor. 148, 150–160, http://dx.doi.org/10.1016/j.gexplo.2014.09.002.
Yang, J., Wang, X., Zhu, M., Liu, H., Ma, J., 2014. Investigation of PAA/PVDF-NZVI hybrids for metronidazole removal: synthesis, characterization, and reactivity characteristics. J. Hazard. Mater. 264, 269–277, http://dx.doi.org/10.1016/j.jhazmat.2013.11.037.
Yarlagadda, S., Gude, V.G., Camacho, L.M., Pinappu, S., Deng, S.G., 2011. Potable water recovery from As, U, and F contaminated ground waters by direct contact membrane distillation process. J. Hazard. Mater. 192 (3), 1388–1394, http://dx.doi.org/10.1016/j.jhazmat.2011.06.056.